Supporting Information

Highly Selective Metal–Organic Framework Textile Humidity Sensor

*Sakandar Rauf,[1] Mani Teja Vijjapu,[1] Miguel A. Andrés,[2, 3] Ignacio Gascón,[2, 3] Olivier Roubeau,[3] Mohamed Eddaoudi[4] and Khaled Nabil Salama[1]**

[1]Advanced Membranes & Porous Materials Centre (AMPMC). Computer, Electrical and Mathematical Sciences and Engineering Division, Sensors Lab. King Abdullah University of Science and Technology (KAUST), Thuwal, 23955-6900, Saudi Arabia.

[2]Departamento de Química Física and Instituto de Nanociencia de Aragón (INA), Universidad de Zaragoza, 50009 Zaragoza, Spain.

[3]Instituto de Ciencia de Materiales de Aragón (ICMA), CSIC and Universidad de Zaragoza, 50009 Zaragoza, Spain.

[4]Functional Materials Design, Discovery & Development Research Group (FMD3) Advanced Membranes & Porous Materials Center, Division of Physical Sciences and Engineering, King Abdullah University of Science and Technology (KAUST), Thuwal 23955-6900, Kingdom of Saudi Arabia.

*Corresponding Author: khaled.salama@kaust.edu.sa

MOF Synthesis and Characterization

MOF NPs of 200 nm (**Figure S1a**) were prepared according to a procedure previously reported in the literature.[1, 2] Briefly, 4.5 g of aluminium nitrate nonahydrate (98.5%, Merck) and 2.52 g of trimesic acid (95%, Sigma Aldrich) were mixed in 300 mL of a H_2O:DMF mixture (volume ratio 1:1). DMF was purchased from Sigma-Aldrich (99.8%). The mixture was reacted for 16 h under reflux with continuous stirring. MOF powder was separated from the obtained white mixture by centrifugation (14500 rpm, 15 min) and washed with deionized water, H_2O:EtOH 1:1 mixture and EtOH. DLS measurements (**Figure S1b**) registered on a Malvern Zetasizer Nano ZSZEN3600 apparatus equipped with a 633 nm laser (reported by some of us in[2]) prove the successful preparation of stable diluted chloroform suspensions with little or no particle agglomeration. Crystalline MOF particles were allowed to dry to the air. The porous structure of this MOF can be described by the presence of three different types of pores: cages with a cavity-free diameter of ca. 11 Å and elongated cavities with approximate dimensions of 9.5 x 12.6 x 11.3 Å (type B) and 3.6 x 4.5 Å (type C). Cavities A are isolated in the structure while cavities B and C are interconnected through microporous windows. Also, there is no connection between cavities of the same type in the framework (i.e., A-A, B-B, C-C).[1, 2]

PXRD (**Figure S1c**) is in good accordance with the simulated pattern proving the crystallinity of the synthesized particles. Band broadening and lower intensities are observed due to the sub-micrometric size. TGA was previously reported[1] using a Perkin Elmer SDA 6000 apparatus and shows a two-step weight loss of water, the first one (25-150ºC) corresponding to the removal of free water molecules trapped in the MOF and the second one (until ca. 300ºC) represents removal

of water molecules coordinated in the framework. Degradation also occurs on a two-step process from 300 to 550ºC.[1]

Water sorption isotherm (registered on a volumetric VStar equipment) was previously reported by some of us[3] and shows a characteristic type I shape in accordance with the microporous nature of the MOF (**Figure S1d**).

ATR-FTIR spectrum (**Figure S1e**) was registered on a Perkin Elmer Spectrum 100 equipment and shows the characteristic symmetric (1660, 1594 cm^{-1}) and asymmetric stretching bands (1457, 1396 cm^{-1}) of coordinated carboxylate groups. The appearance of two bands for each vibration mode suggests the presence of two different carboxylate groups in the MOF. C-O asymmetric stretching (1116 cm^{-1}), aromatic C=C skeletal vibration (1633 cm^{-1}), and –OH deformation bands (1067, 957 cm^{-1}) can also be observed.

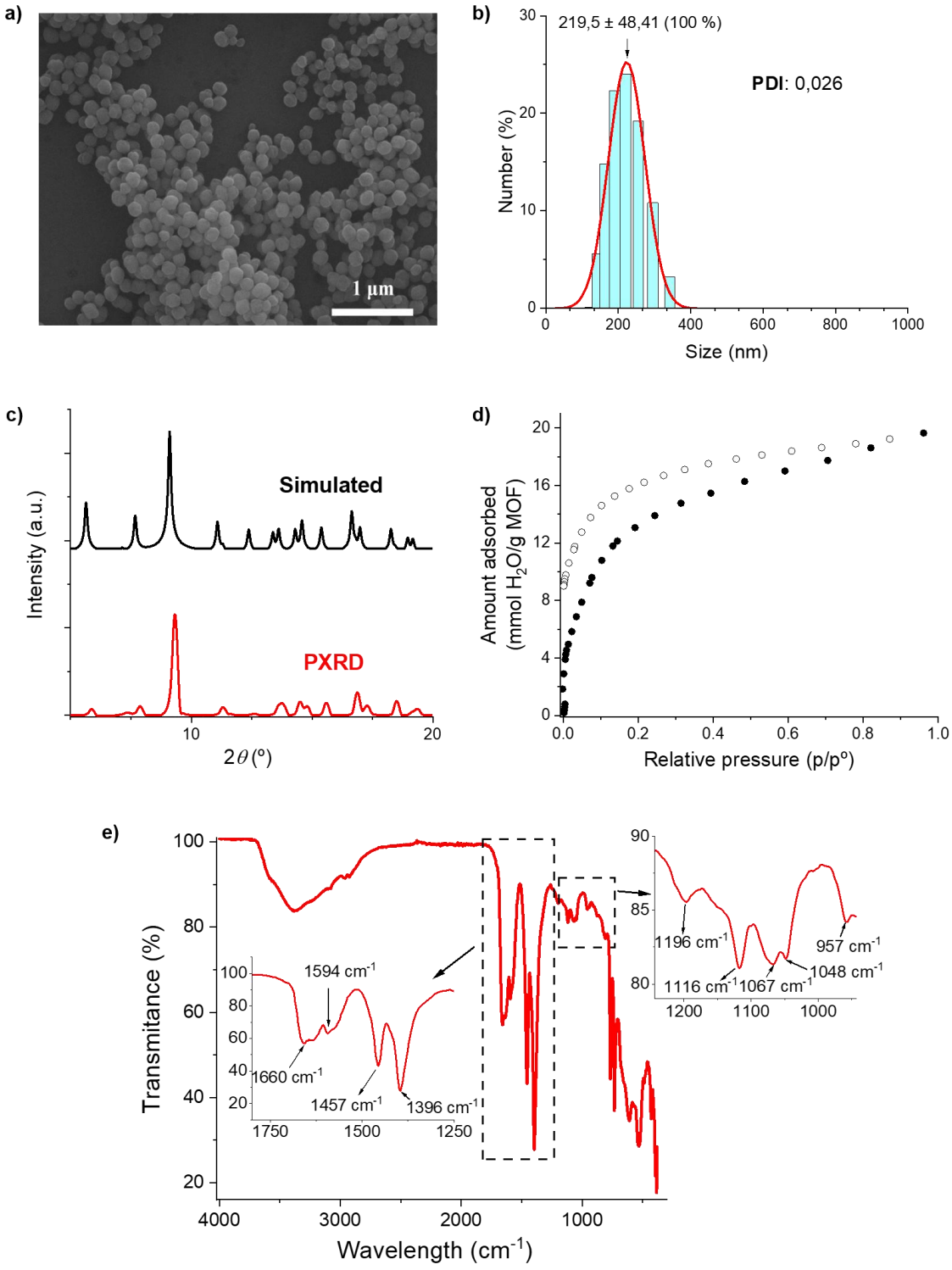

Figure S1: (a) SEM image of MOF NPs. (b) DLS measurements of an ultrasonicated 0.2 mg/mL suspension in chloroform. (c) PXRD of MOF NPs. A simulated pattern derived from the crystalline structure[1] is also shown for comparison purposes. (d) Water sorption isotherm registered on a volumetric equipment (VStar). Activation conditions: 16 h 150ºC under vacuum (10^{-3} mbar). (e) ATR-FTIR spectrum of MOF powder showing the characteristic absorption bands.

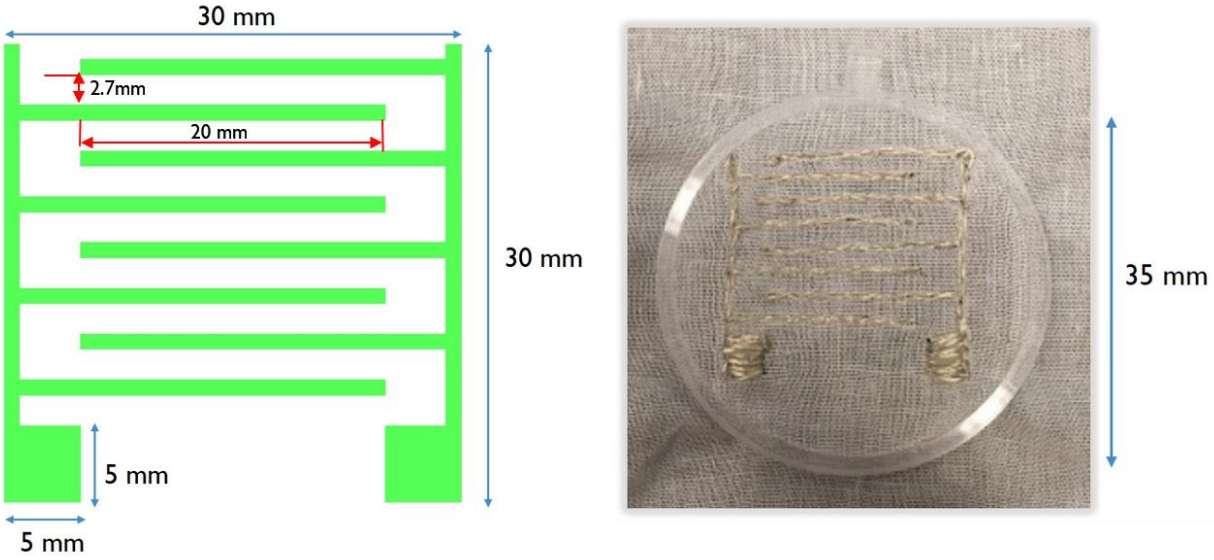

Figure S2: (left) Schematic representation of the patterned dimensions of the interdigitated electrodes. (right) Photograph showing one TEX sensor inside a PMMA holder ready for the deposition of the MOF layer. The extra cloth was cut from the holder before the deposition.

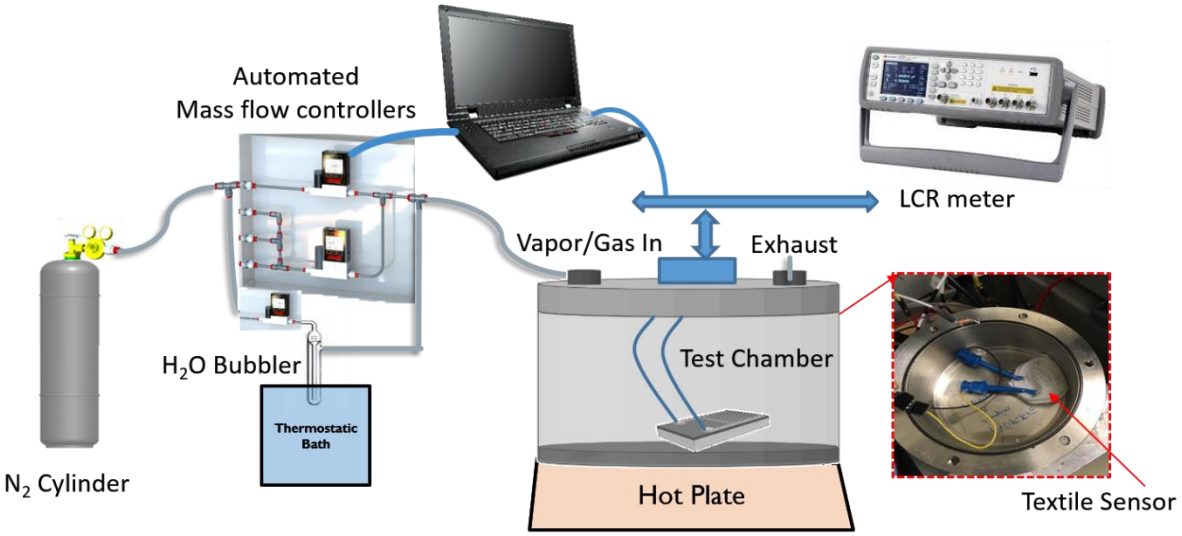

Figure S3: Schematic representation of the experimental setup used for the measurement of humidity using the MOF coated interdigitated textile electrodes.

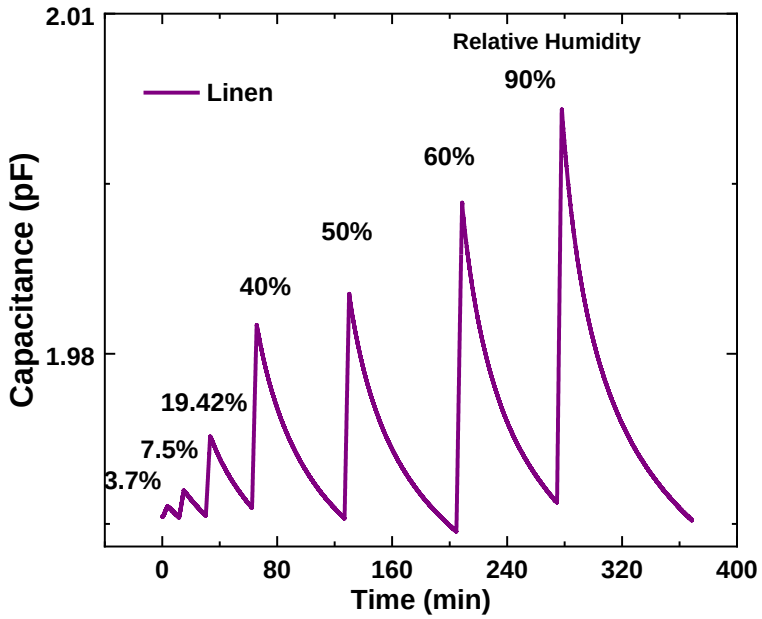

Figure S4: Shows the absolute capacitance change in the TEX sensor in presence of humidity with baseline capacitance of 1.97 pF. Relative humidity was measured at 22 ºC.

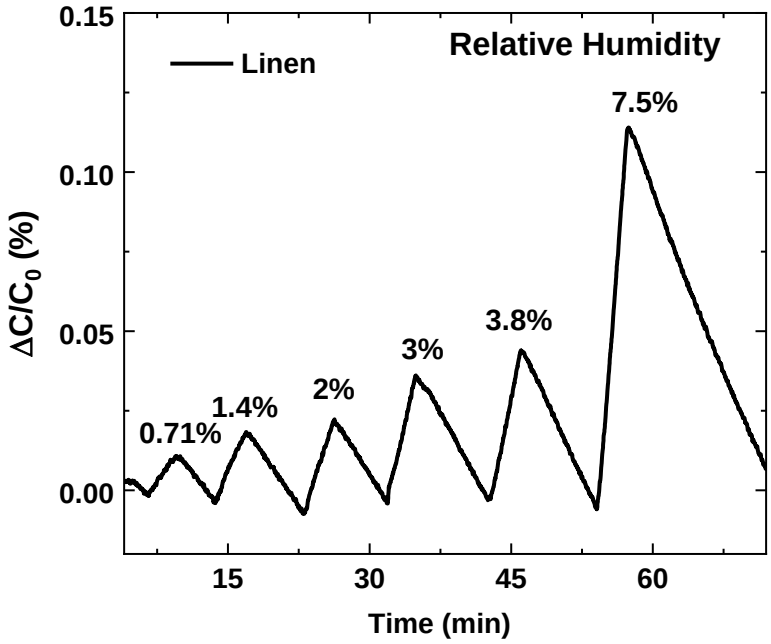

Figure S5: Responsivity of the linen textile sensor showing the variation in capacitance for water vapor concentrations ranging from 0.71% to 7.5% relative humidity. Sensitivity values are expressed as ΔC/C (%). Relative humidity was measured at 22 ºC.

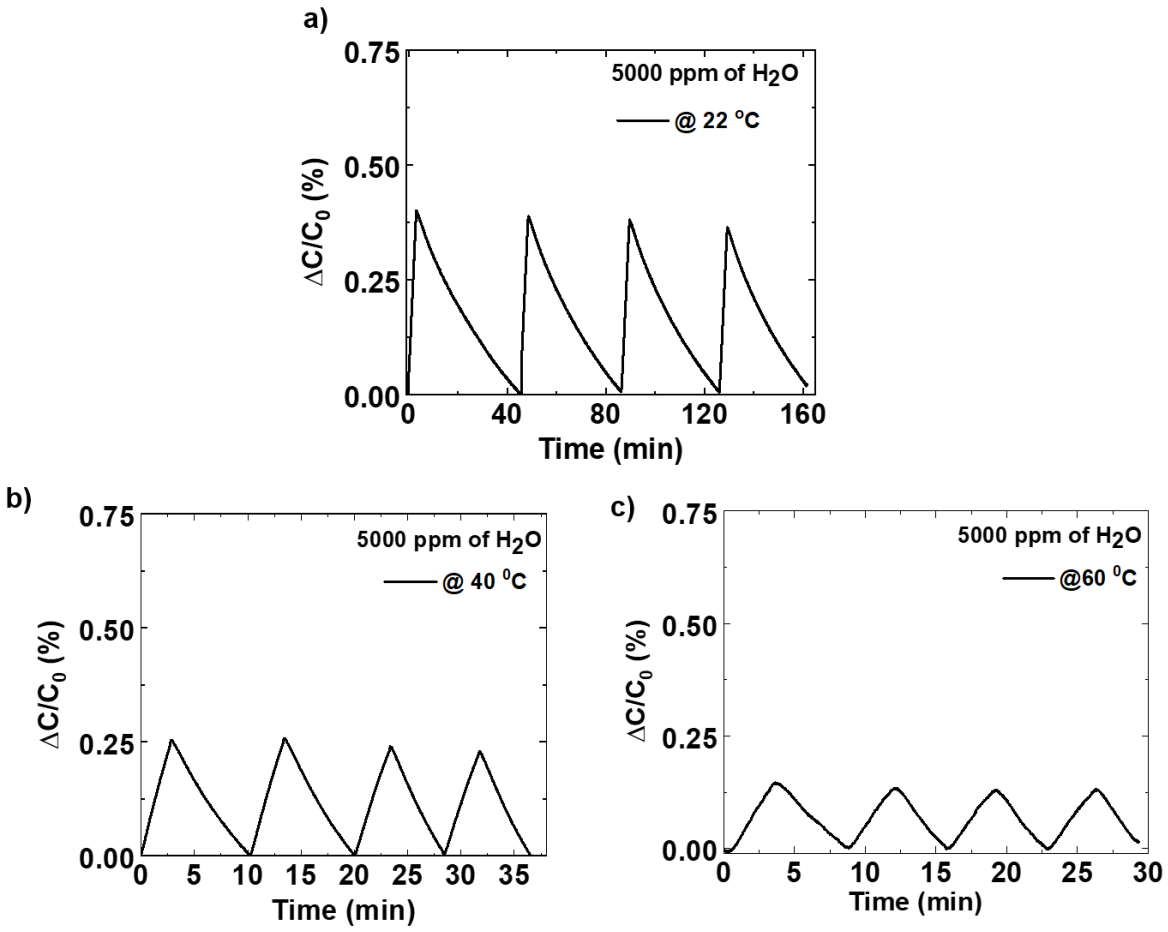

Figure S6: Capacitive response curves for recycling experiments performed on linen TEX sensor at 5000 ppm of water vapor at different temperatures: (a) room temperature (22 °C) (b) 40 °C and (c) 60 °C.

Table S1. Humidity Sensors

Sensing platform	Transducer type	Active material	Range (RH %)	Sensitivity (per %RH)	Selectivity	Response type	Refs
Solid state	IDE Cap	GO + ZnO	15-95	50 ($\Delta C/C*100$)	NR	Non-linear	4
Solid state	IDE Cap	T-crystals	5-95	1.5($\Delta C/C*100$)	Good	Non-linear	5
Solid state	MIM Cap	TiO_2 + Polymer	10-90	0.3 ($\Delta C/C*100$)	NR	Linear	6
Solid state	MEMS Cap	Poly-imide	30-80	0.051 ($\Delta C/C*100$)	NR	Non-linear	7
Solid state	Resistive	M-Xene	30-100	3.3 ($\Delta C/C*100$)	Poor	Non-linear	8
Solid state	IDE Cap	MIL-96(Al) MOF +Parlyene-C	0.4-90	0.008 ($\Delta C/C*100$)	Good	Linear	9
Solid state	Parallel Plate Cap	SIM	10-90	--	Good	Non-linear	10
Membrane	Resistive	NFC composite	11-95%	0.33 ($\Delta R/R*100$)	Poor	Linear	11
Membrane	Parallel Plate Cap	Graphene + PVDF	40-100	0.07 ($\Delta R/R*100$)	NR	Non-linear	12
Paper	IDE Cap	Paper	40-100	3.5 ($\Delta C/C*100$)	NR	Non-linear	13
Fiber	Resistive	SWCNT+PVA	60-100	1.3 ($\Delta R/R*100$)	NR	Non-linear	14
Thin-film	Resistive	NFC/CNT	11-95	0.78 ($\Delta I/I*100$)	NR	Linear	15
Fabric	Resistive	MWCNTs/Cotton	55-95	-----	NR	Non-linear	16
Fabric	Impedance	Nafion	50-95	-1.05% ($\Delta Z/Z*100$)	NR	Linear	17
Fabric	IDE Cap	MIL-96(Al) MOF	0.71 - 90	0.02 ($\Delta C/C*100$)	Good	Linear	This work

GO: graphene oxide, T-Crystals: trianglamine hydrochloride crystals, PVA: poly(vinyl alcohol), SWCNT: single walled carbon nanotubes, MWCNTs: multi walled carbon nanotubes, SIM: supramolecular ionic materials, NFC: nanofiber composite, CNT: carbon nanotubes, NR: not reported, IDE: Inter digitated electrodes, MIM: metal Insulator metal, Cap: capacitance, MEMS: micro-electromechanical systems

References

1. Benzaqui, M.; Pillai, R. S.; Sabetghadam, A.; Benoit, V.; Normand, P.; Marrot, J.; Menguy, N.; Montero, D.; Shepard, W.; Tissot, A.; Martineau-Corcos, C.; Sicard, C.; Mihaylov, M.; Carn, F.; Beurroies, I.; Llewellyn, P. L.; De Weireld, G.; Hadjiivanov, K.; Gascon, J.; Kapteijn, F.; Maurin, G.; Steunou, N.; Serre, C., Revisiting the Aluminum Trimesate-Based MOF (MIL-96): From Structure Determination to the Processing of Mixed Matrix Membranes for CO_2 Capture. *Chem Mater* **2017,** *29* (24), 10326-10338.

2. Andres, M. A.; Benzaqui, M.; Serre, C.; Steunou, N.; Gascon, I., Fabrication of ultrathin MIL-96(Al) films and study of CO_2 adsorption/desorption processes using quartz crystal microbalance. *J Colloid Interf Sci* **2018,** *519*, 88-96.

3. Andres, M. A.; Vijjapu, M. T.; Surya, S. G.; Shekhah, O.; Salama, K. N.; Serre, C.; Eddaoudi, M.; Roubeau, O.; Gascon, I., Methanol and Humidity Capacitive Sensors Based on Thin Films of MOF Nanoparticles. *Acs Appl Mater Inter* **2020,** *12* (3), 4155-4162.

4. Li, X. Y.; Chen, X. D.; Chen, X. P.; Ding, X.; Zhao, X., High-sensitive humidity sensor based on graphene oxide with evenly dispersed multiwalled carbon nanotubes. *Mater Chem Phys* **2018,** *207*, 135-140.

5. Chappanda, K. N.; Chaix, A.; Surya, S. G.; Moosa, B. A.; Khashab, N. M.; Salama, K. N., Trianglamine hydrochloride crystals for a highly sensitive and selective humidity sensor. *Sensors and Actuators B: Chemical* **2019,** *294*, 40-47.

6. Liu, M.-Q.; Wang, C.; Kim, N.-Y., High-Sensitivity and Low-Hysteresis Porous MIMType Capacitive Humidity Sensor Using Functional Polymer Mixed with TiO_2 Microparticles. *Sensors (Basel, Switzerland)* **2017,** *17* (2), 284.

7. Chen, S. C.; Chung, V. P. J.; Yao, D. J.; Fang, W. In *Vertically integrated CMOS-MEMS capacitive humidity sensor and a resistive temperature detector for environment application*, TRANSDUCERS 2017 - 19th International Conference on Solid-State Sensors, Actuators and Microsystems, 2017; pp 1453-1454.

8. Yang, Z.; Liu, A.; Wang, C.; Liu, F.; He, J.; Li, S.; Wang, J.; You, R.; Yan, X.; Sun, P.; Duan, Y.; Lu, G., Improvement of Gas and Humidity Sensing Properties of Organ-like MXene by Alkaline Treatment. *ACS Sensors* **2019,** *4* (5), 1261-1269.

9. Andrés, M. A.; Vijjapu, M. T.; Surya, S. G.; Shekhah, O.; Salama, K. N.; Serre, C.; Eddaoudi, M.; Roubeau, O.; Gascón, I., Methanol and Humidity Capacitive Sensors Based on Thin Films of MOF Nanoparticles. *ACS Applied Materials & Interfaces* **2020,** *12* (3), 4155-4162.
10. Yan, H.; Zhang, L.; Yu, P.; Mao, L., Sensitive and Fast Humidity Sensor Based on A Redox Conducting Supramolecular Ionic Material for Respiration Monitoring. *Analytical Chemistry* **2017,** *89* (1), 996-1001.
11. Huang, X.; Li, B.; Wang, L.; Lai, X.; Xue, H.; Gao, J., Superhydrophilic, Underwater Superoleophobic, and Highly Stretchable Humidity and Chemical Vapor Sensors for Human Breath Detection. *ACS Applied Materials & Interfaces* **2019,** *11* (27), 24533-24543.
12. Hernández-Rivera, D.; Rodríguez-Roldán, G.; Mora-Martínez, R.; Suaste-Gómez, E., A Capacitive Humidity Sensor Based on an Electrospun PVDF/Graphene Membrane. *Sensors* **2017,** *17* (5).
13. Gaspar, C.; Olkkonen, J.; Passoja, S.; Smolander, M., Paper as Active Layer in Inkjet-Printed Capacitive Humidity Sensors. *Sensors* **2017,** *17* (7).
14. Zhou, G.; Byun, J.-H.; Oh, Y.; Jung, B.-M.; Cha, H.-J.; Seong, D.-G.; Um, M.-K.; Hyun, S.; Chou, T.-W., Highly Sensitive Wearable Textile-Based Humidity Sensor Made of High-Strength, Single-Walled Carbon Nanotube/Poly(vinyl alcohol) Filaments. *ACS Applied Materials & Interfaces* **2017,** *9* (5), 4788-4797.
15. Zhu, P.; Liu, Y.; Fang, Z.; Kuang, Y.; Zhang, Y.; Peng, C.; Chen, G., Flexible and Highly Sensitive Humidity Sensor Based on Cellulose Nanofibers and Carbon Nanotube Composite Film. *Langmuir* **2019,** *35* (14), 4834-4842.
16. Rosace, G.; Trovato, V.; Colleoni, C.; Caldara, M.; Re, V.; Brucale, M.; Piperopoulos, E.; Mastronardo, E.; Milone, C.; De Luca, G.; Plutino, M. R., Structural and morphological characterizations of MWCNTs hybrid coating onto cotton fabric as potential humidity and temperature wearable sensor. *Sensor Actuat B-Chem* **2017,** *252*, 428-439.
17. Weremczuk, J.; Tarapata, G.; Jachowicz, R., Humidity sensor printed on textile with use of ink-jet technology. *Procedia Engineer* **2012,** *47*, 1366-1369.